Study of Real Defects on EUV Blanks and a Strategy for EUV Mask Inspection

Sungmin Huh[1], Abbas Rastegar[1], Stefan Wurm[1], Kenneth Goldberg[2], Iacopo Mochi[2],
Toshio Nakajima[3], Masahiro Kishimoto[3], Mitsuhiko Komakine[3]

[1] SEMATECH 255 Fuller Road, Suite 309, Albany, NY 12203 USA
[2] 2-400, Lawrence Berkeley National Laboratory, Berkeley, CA 94720
[3] AGC Electronics America , 257 Fuller Road, Albany NY 12203

ABSTRACT

The availability of defect-free masks remains one of the key challenges for inserting extreme ultraviolet lithography (EUVL) into high volume manufacturing, yet little data is available for understanding native defects on real masks. In this paper, two EUV mask blanks with known native buried phase defects were characterized with a Lasertec M7360 (266 nm wavelength), atomic force microscope (AFM), and SEMATECH's actinic inspection tool (AIT), which is an EUV-wavelength microscope. The results show that there are various kinds of native defects on the mask blank. Not surprisingly, the surface height and measured EUV intensity profile of real blank defects can differ significantly from Gaussian-shaped defects. All defects found by the M7360 were observable in the AIT, yet many do not perturb the intensity enough to be printable in isolation. This paper shows that defects come in various sizes and types and clarifies what must be done to learn more about real defect printability to achieve defect-free mask blanks.

Keywords: EUV, mask, phase defect, Confocal DUV inspection, actinic inspection

1. INTRODUCTION

Over the past year, leading-edge chip manufacturers have shifted their interest towards the insertion of extreme ultraviolet lithography (EUVL). This emphasis is increasing the pressure to resolve defect-free blanks, which remains one of the key challenges impeding EUVL insertion into high volume manufacturing (HVM). The success of the industry's mask blank defect reduction effort critically depends on the timely availability of inspection tools that can precisely and reliably find ever smaller defects. SEMATECH's Mask Blank Development Center (MBDC) has provided the world's best defect inspection capability starting in 2003 with the Lasertec M1350 tool and continuing with the second generation tool, the M7360, in 2006. Both tools have deep ultraviolet (DUV) light sources for defect detection: 488 nm wavelength for the M1350 and 266 nm wavelength for the M7360. However, to meet high volume manufacturing requirements for sub-32 nm half-pitch (HP) patterning, the industry needs a blank inspection tool to determine printability in the EUV wavelength (13.5 nm). SEMATECH operates and funds an EUV-wavelength microscope (the SEMATECH actinic inspection tool [AIT] at Lawrence Berkeley National Lab [LBNL]) and a state-of-the-art Lasertec M7360 to support the development of inspection tools and reticle blanks to eventually meet HVM requirements. In this paper, two EUV mask blanks with known native buried phase defects were characterized with a Lasertec M7360 (266 nm wavelength), atomic force microscope (AFM), and AIT. Our results show that there are various kinds of native defects on the mask blank. Not surprisingly, the surface height and measured EUV intensity profile of real blank defects can differ significantly from the intensity drop of Gaussian-shaped defects. All defects found by the M7360 were observable in the AIT, yet many do not perturb the intensity enough to be printable in isolation. This paper shows defects come in many sizes and types and clarifies what must be done to learn more about real defect printability to achieve defect-free mask blanks.

2. DEFECT ON EUV BLANK AND INSPECTION TOOL

Three types of defects can be found on the blank level of an EUV mask: surface pits, which originate from the substrate pits that decorate during multilayer deposition; bumps or covered particles, which originate from embedded substrate particles or mechanical walk particles; and covered or partially covered defects added by the multilayer deposition process. Figure 1 shows defect types on the substrate and blank. Pit defects are most dominant, accounting for on average 75% of the defects observed. Embedded particles on the substrate can be cleaned by advanced cleaning process. The remaining 25% of defects are due to particles deposited during the deposition process [1]. Figure 2 shows the EUV mask fabrication flow and the required metrology and inspection tools. A blank inspection tool, patterned mask inspection tool, and defect inspection using actinic wavelength (EUV AIMS) are needed to qualify the mask. However, an EUV AIMS is not currently available. Furthermore, it appears that this tool will not be available even for pilot line or early HVM operation. Consequently, wafer inspection must be done after wafers are printed.
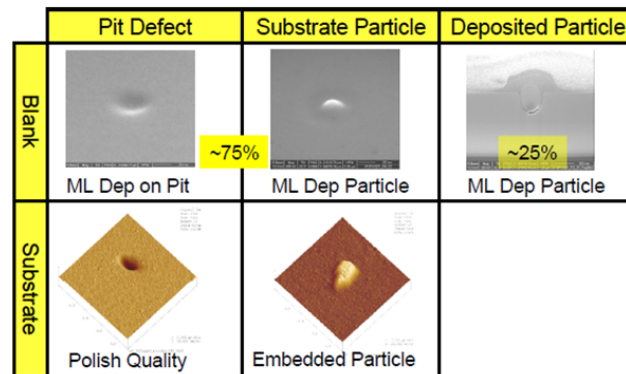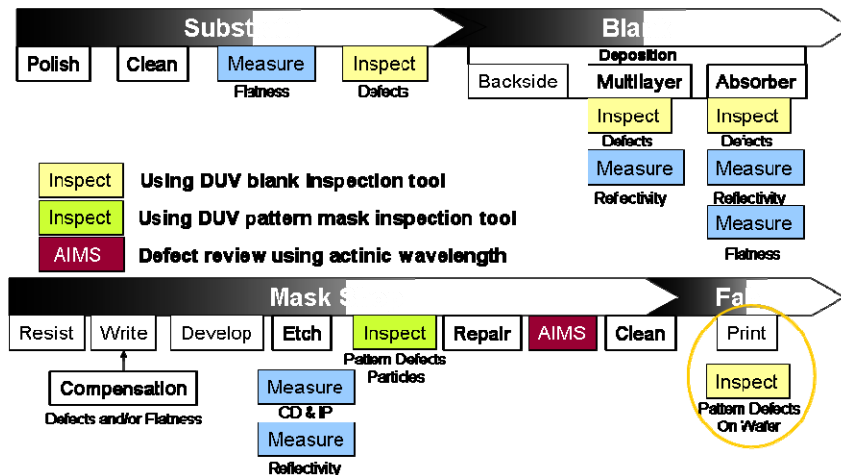

Figure 1. Types of defects on an EUV blank

Figure 2. EUV mask fabrication flow for timing of pilot line application or early HVM

3. EXPERIMENTAL

3.1 Experimental procedure

Two EUV blanks from SEMATECH's Mask Blank Development Center (MBDC) and a commercial blank shop were prepared for this study. The native buried phase defects were inspected with the M7360 and AFM at SEMATECH. Twenty-six defects on each blank were chosen for defect review with the AIT to understand whether or not all defects detected by the DUV blank inspection tool are printable in the actinic wavelength of the EUV AIMS or EUV scanner.

An experimental plan is shown in Figure 3. SEMATECH has operated the AIT as a defect review and imaging tool at LBNL (see Figure 4). The AIT is a Fresnel zoneplate microscope that projects a highly magnified image of the light reflected from a mask's surface onto an EUV charge coupled device (CCD) camera. A closely spaced array of zoneplates enables the user to select from objective lenses with different optical properties. In this way, the AIT can emulate the spatial resolution of various existing and future EUV lithography tools. For example, with 0.0625, 0.0750, and 0.0875 numerical aperture (NA) objectives, the AIT emulates 4X demagnification projection tools with a 0.25, 0.30, or 0.35 NA, beyond the current state of the art. For the zoneplates now installed in the AIT, the magnification ratio is 907; the 13.5 μm square pixels on the CCD camera correspond to a 15 nm square area on the mask surface. This pixel density is several times higher than the resolution of the AIT to allow appropriate sampling of the image. The AIT's imaging parameters are detailed in Table 1 [2-4].

For the analysis of AIT images to emulate defect printability in wafer scale,

- Defect size (wafer)=Defect size (AIT) / 4

- Focus (wafer)=Focus (AIT) / 16

- "0 nm" focusing is on top of the multilayer. "+" focusing beam to the vacuum. "–" focusing beam to the multilayer

- AIT illumination has σ ~ 0.15, which is a higher coherent than the scanner. Defects will be less printable at a high σ in the scanner

- NA of AIT=0.35 in wafer scale

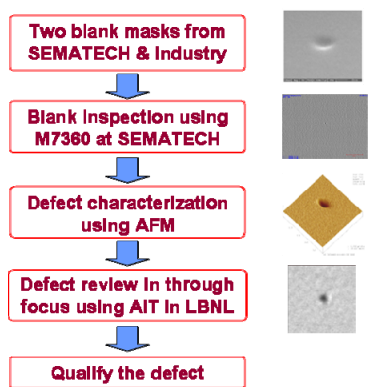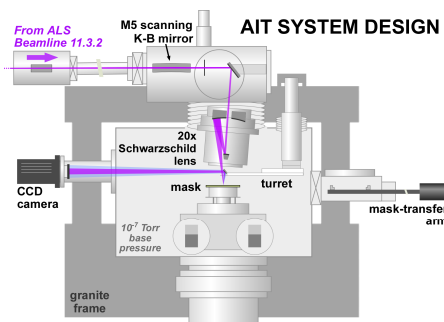Figure 3. Experimental procedure

Figure 4. AIT system design

Table 1. AIT imaging parameters.

Property	Value
Wavelength	13.4 ± 0.01 nm, tunable
available NA values	{0.25, 0.30, 0.35} (4×) {0.0625, 0.075, 0.0875} (1X)
zoneplate focal length(s)	680, 750, 1000 μm
Magnification	680, 907, 1000×
observable mask area	~ 31 μm for 907×
high-quality field of view	~ 2–8 μm, dependent on feature size.
Typical data collection rate	approx. 250 images / 8h

3.2 Test blanks for real defect printability

The 52 chosen defects, 26 on each blank, were analyzed for inspection capability and printability. Figure 5 shows a Pareto chart of those defects on each blank based on AFM results. All defects were measured with the AFM for profile information such as full width at half maximum (FWHM) and depth or height (see Figure 6). Most defects found were pits, which is shown in Figure 1. While much smaller defects are likely to be on the mask blank, we could get no information on defects smaller than the sensitivity of M7360. This paper focuses on the characterization of defect printability in clear field, not with the pattern. The printability criteria of defects are based on simulation results as a function of defect size and height for the 32, 22, and 16 nm nodes [5]. Possible parameters such as NA and illumination are considered for each critical dimension (CD) node in Table 2. We can find the intensity threshold to define the CD for each node. If the intensity drops by more than 60% (i.e., to a 0.4 intensity threshold in Figure 7), then the defect has the potential to be printed on the wafer (Figure 6(a)). However, when the intensity drop is less than 60%, the defect will not print (Figure 6(b).) As we can see in Table 2, most intensity loss thresholds for printable defects are near 0.4 at various pitches and CDs. This is because of the large k_1 factor of EUV lithography. Consequently for this study, the printable intensity threshold was set at 0.4. For example, if the minimum intensity is less than 0.4 of the intensity threshold, we considered this a defect that would print on the wafer. The two defects in Figure 6 have the same pixel numbers in the M7360, but show different printability in the EUV wavelength (13.5 nm). This means that for EUVL to be successful, an actinic inspection tool and EUV AIMS should be developed. Otherwise, we will need to correlate the defect printability in an actinic inspection tool and DUV inspection tool, meaning we must detect all defects on the blank regardless of how they appear in the substrate and blank inspection tool.
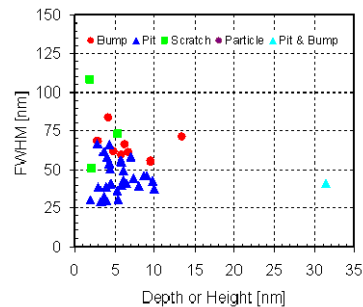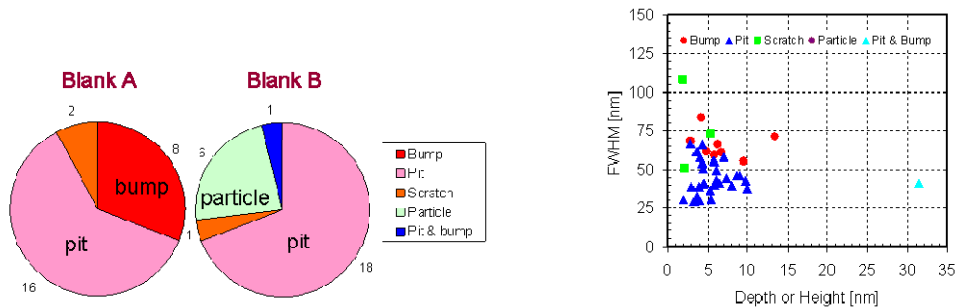

Figure 5. Pareto chart of defects in 2 test blanks   Figure 6. Defect profile of each defect using the AFM

Table 2. Simulation conditions and intensity threshold values

Property	Illumination condition	NA	Intensity threshold
32nm 1:1	Conventional, σ : 0.5	0.25	0.39
22nm 1:1	Annular, σ : 0.3/0.5	0.35	0.395
16nm 1:1	Annular, σ : 0.3/0.5	0.45	0.39
21nm 1:2	Conventional, σ : 0.5	0.25	0.37
15nm 1:2	Annular, σ : 0.3/0.5	0.35	0.38
11nm 1:2	Annular, σ : 0.3/0.5	0.45	0.39
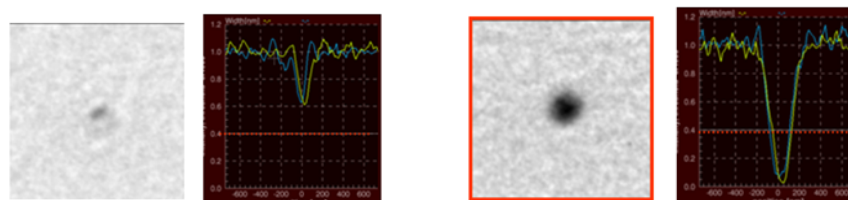
(a) Unprintable blank defect   (b) Printable blank defect

Figure 7. Example of a printable and unprintable blank defect

4. RESULTS AND DISCUSSION

4.1 The type of real defect on EUV blank

Figure 8 shows the various kinds of phase defects observed in the 52 defect signatures after AIT and AFM evaluation. Various kinds of defects are seen on the EUV blank. Some of them are not Gaussian-shaped, but arbitrarily shaped. The real blank defects have various profiles that are different from programmed or simulated defects, which were investigated in previous studies. Most defect profiles of simulated or programmed defects are Gaussian-shaped pits or bumps [6]. For example, a big scratch (larger than hundreds of nm) is almost unprintable in the AIT. The level of intensity drop is almost at noise level. This means that this kind of defect would be unprintable on the wafer using the ADT. Pit defects get more printable at "-" defocus, while bumps get more printable at "+" defocus (see Figure 9). This means that through-focus defect inspection with the actinic inspection tool needs to detect bumps and pits at the same time. However, through-focus inspection will increase the total inspection time. Figure 10 shows that printability can be different even if the defect size is similar. The difference in depth is only 0.2 nm and in size is 10 nm on the mask scale (2.5 nm on the scanner scale). However, the intensity drop of the two defects in the AIT images is vastly different. The main reason for this difference is still unknown. It is speculated that the edge profile of defects affects printability.
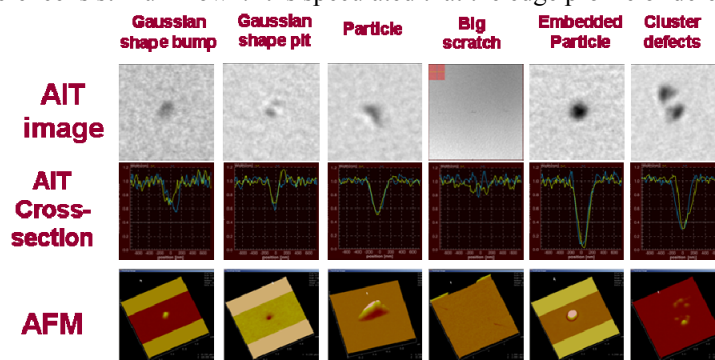

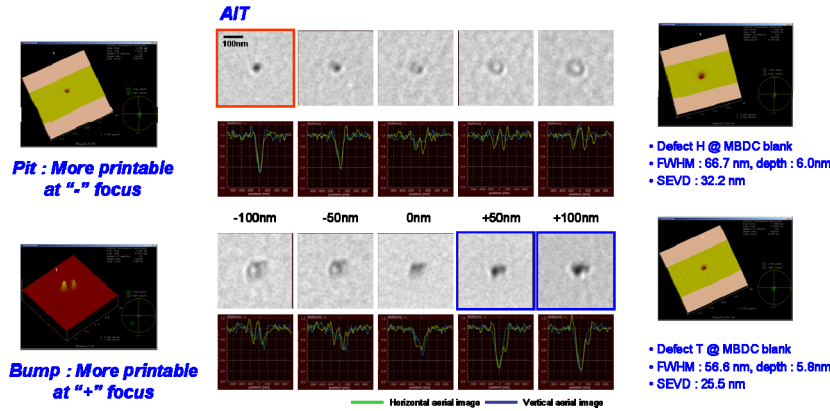Figure 8. Examples of real defects from the AIT and AFM

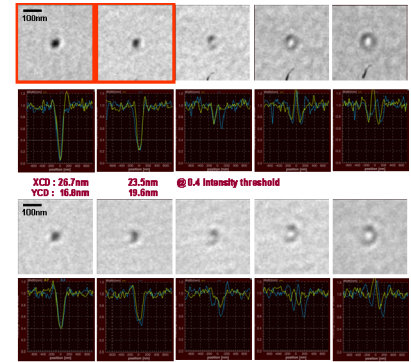Figure 9. Printability as through-focus of bumps and pits

Figure 10. Printability of defects of similar sizes and pit defects

4.2 Defect printability as through-focus

Phase defects are very sensitive to the focal plane on the wafer. The mask focal planes were split into -50 nm, best focus, +50 nm in the AIT images to determine the focus dependency of phase defects. The least printable at best focus is shown in Figure 11 (b). There is also a correlation between printability and defect profile. This means that most defects have different profiles in the EUV wavelength. Pits are more printable at a defocus of "-50 nm." Bumps become more printable at a defocus of "+50 nm." The probability of printable defects at the intensity threshold of 0.4 is listed in Table 3.
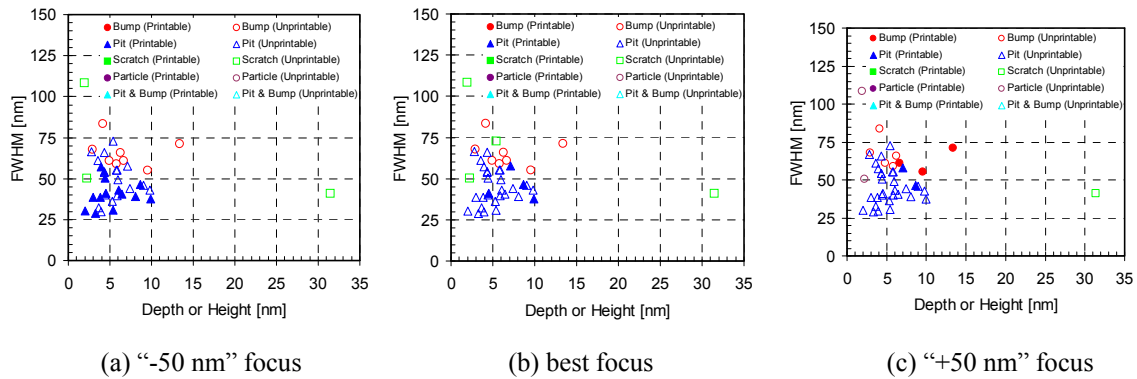

(a) "-50 nm" focus   (b) best focus   (c) "+50 nm" focus

Figure 11. Defect printability as through-focus

Table 3. The printability of defects in various focal planes

Focal plane	% of printability
"-50 nm" focus	36.3%
Best focus	13.6%
"+50 nm" focus	9%

4.3 Defect inspection and review procedure

We need to fully quantify the effect of using various inspection tools on EUV masks. An actinic blank inspection tool must be able to fully quantify the printability of each defect. However, we may not need actinic inspection if a DUV blank inspection tool can have sensitivity comparable to an actinic inspection tool. We do need to find all defects on a blank regardless of what they are; we need their exact location; we need to quantify their aerial image; and finally we must decide which blanks must be discarded or can be repaired or where smart pattern placement can help. A printability database providing the correlation between optical and actinic imaging would help blank manufacturers determine whether defects have a printable signature or not. If there are defects on the EUV blank, we need to quantify their aerial image, size, and location and use the blank in the mask shop. Mask shops need to sort for the layer used by the number of defects. For example, a blank with many defects can be used for the contact layer, while one with few defects should be used for the gate poly layer. Defect review using an AIMS or wafer inspection tool should be used to qualify the final mask. A possible mask fabrication flow using defect mitigation technology is shown in Figure 12.
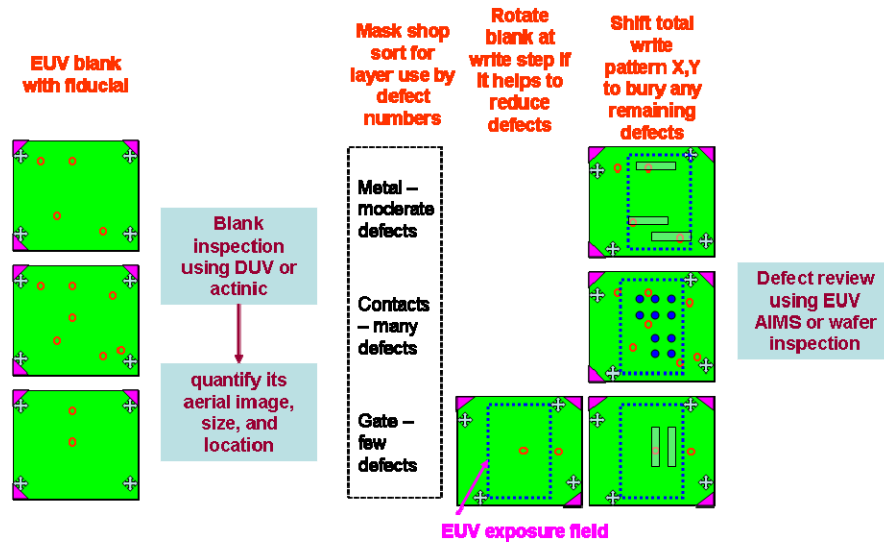

Figure 12. Strategy of defect mitigation for EUV masks

5. CONCLUSION AND FUTURE WORK

Reducing defects on EUV mask blanks is a key technology for EUV lithography when used in mass production. SEMATECH, in collaboration with industry, is evaluating defect printability on EUV masks using the ADT, AIT, and wafer inspection. In this paper, we studied phase defect printability for the 32/22/16 nm half-pitch, specifically real defect printability on the mask blank at through-focus using the AIT. The printability on mask blanks is very sensitive to the focus. Pits and bumps have the opposite defect printability at through-focus. Not all defects detected by the M7360 have enough of an intensity drop in the AIT. This means they will not print on the wafer. We need to further study defect printability considering resist performance. We need more realistic specifications for defects on EUV masks if EUV lithography is to be successful in high volume manufacturing.

REFERENCES

1. Yun, H., Goodwin, F., Huh, S., Orvek, K., Cha, B., Rastegar, A., Kearney, P., "SEMATECH EUVL mask program status," Proceedings of SPIE Vol. 7379, 73790G (2009).
2. K. A. Goldberg, A. Barty, Y. Liu, P. Kearney, Y. Tezuka, T. Terasawa, J. S. Taylor, H. S. Han, and O. R. Wood II., J. Vac. Sci. & Technol. B 24 (6), 2824 (2006).
3. K. A. Goldberg, P. P. Naulleau, A. Barty, S. B. Rekawa, C. D. Kemp, R. F. Gunion, F. Salmassi, E. M. Gullikson, E. H. Anderson, H. S. Han, Proc. SPIE 6730, 67305E (2007).

4. K. A. Goldberg, S. B. Rekawa, C. D. Kemp, A. Barty, E. H. Anderson, P. Kearney, H. S. Han, Proc. SPIE 6921, 69213U (2008).
5. Huh, S., Kearney, Kearney, P., Wurm, S., Goodwin, F., Han, H., Goldberg, K., Mochi, I., Gullikson, E., "EUV actinic defect inspection and defect printability at the sub-32-nm half-pitch," Proceedings of SPIE Vol. 7470, 74700Y (2009).
6. Stefan Wurm, Hakseung Han, Patrick Kearney, Wonil Cho, Chan-Uk Jeon, and Eric Gullikson, Proc. SPIE 6607, 66073A, (2007).